Electronic Supplementary Material (ESI) for ChemComm.

Supplementary Information

Synergetic impact of high-entropy microdoping modification in $Na_3V_2(PO_4)_3$

Yahao Kang,[a] Xitao Lin,[b] Shuai Tong,[a] Wenlong Zhu,[a] Yang Wang,[a] Min Jia*[a] and Xiaoyu Zhang *[a]

a. School of Material Science and Engineering, Jiangsu University, Zhenjiang 212013, China.

E-mail: x.zhang@ujs.edu.cn

b. Key Lab for Advanced Materials and Clean Energies of Technologies, Southwest University, Chongqing 400715, P. R. China,

Experimental section

Materials synthesis

High entropy $Na_3V_{1.9}(Ca,Mg,Cr,Ti,Mn)_{0.1}(PO_4)_3/C$ was synthesized via traditional high temperature solid-phase reaction.Firstly,Na_2CO_3,V_2O_5 and $NH_4H_2PO_4$ in a calculated stoichiometric ratio was mixed uniformly in a planetary balling machine.Then, CaO,MgO,Cr_2O_3,TiO_2 and MnO_2 with the equal of 0.02 mole were added in turn. Finally, 5wt% of Acetylene black was added for milling for 8h at 400 rpm.After that,the precursor mixture was ground into powder and calcined at 300 °C for 5 h then 800 °C for 10h with the heating rate of 5 °C/min in an H_2(5%)/Ar atmosphere to obtain $Na_3V_{1.9}(Ca,Mg,Cr,Ti,Mn)_{0.1}(PO_4)_3/C$ (marked as HE-$NV_{1.9}$MP). For comparison,the $Na_3V_2(PO_4)_3/C$ was fabricated with the same method mentioned above without adding the doping elements (marked as NVP).

Materials Characterization

The crystal structure of HE-$NV_{1.9}$MP was studied through X ray diffraction (XRD) using a Smartlab SE Advance Diffractometer (Cu-Kα radiation, λ = 1.5418 Å, current: 30 mA, voltage: 40 kV) in the scan range (2θ) of 10° - 80°. And the GSAS software was used for the XRD date analysis. In-situ XRD test was carried out at a current density 30mA g^{-1} in in-situ cell with the Be disk as test window. The morphology and microstructure of sample was researched using scanning electron microscopy (SEM) ((FEI NovaNano 450) and transmission electron microscopy (JEOL 2100 PLUS). X-ray photoelectron spectroscopy (XPS) measurements were carried out on a Thermo Scientific K-Alpha instrument equipped with a monochromatic Al-Kα source.

Electrochemical Measurements

To further evaluating the electrochemical performance of the samples, the Na half cells and full cells were assembled. The cathode electrodes, which were made up of 70 wt% of active material, 20 wt% of acetylene black and 10 wt% polyvinylidene fluoride (PVDF) accompanied with proper amount of N-methyl-2-pyrrolidone (NMP) solvent, were cast on Al foil. The loading mass of active materials of the electrodes was limited in the range of 1.0 - 1.2 mg cm^{-2}. And Na metal was used for the counter electrode for Na half cells. Corresponding, 85 wt% of hard carbon, 15 wt% acetylene black and 5 wt% sodium alginate were mixed up with deionized water, which was coated on Al foil. And then the electrodes were dried at 80 °C overnight in a vacuum oven, and rolled and

sliced to produce the positive electrode sheet. The CR2032-type coin cells were assembled in a pure argon filled glove box. 1M $NaClO_4$ in PC with 5vol% FEC used as electrolyte and the glass fiber membrane (Whatman) used for separator. The assembled battery was then left to stand for 10 h. The LandBT2001A battery test system was selected for electrochemical testing with a voltage window of 2.5−4.3 V. A constant current intermittent titration test (GITT) was performed with a current density of 10 mA g^{-1}, taking a pulse time of 30 min and a relaxation time of 4 h for the first two cycles. And Cyclic voltammetry (CV) tests were performed on an electrochemical workstation (ChenHua Instruments, Inc., Model CHI 760E).

In order to match the cathode/anode capacity, the anode capacity in excess of cathode, and the mass ratio of HC to HE-$NV_{1.9}$MP was about 1:1.7. The voltage window for the full cell is within 2.3-4.1V. The calculation of the specific capacity of the full cell was based on the mass of the cathode active material.

Material Design

Considering the dopant radius, Zhao et. al.[1] prepared Ca^{2+} doped NVP with the expanded lattice space due to the large radium of Ca^{2+} (1.0 Å) compared with V^{3+} (0.69 Å) which greatly improved the stability of NVP. Wang et. al.[2] introducing Mg^{2+} in the NVP which successfully acted as pillars to prevent the structure collapse upon cycling and improved the electrochemical performance.

To activate the V^{4+}/V^{5+} redox couple, Mn[3] and Cr[4] substitutions were proposed to achieving the better stability at the high operating voltage. However, the irreversible phase transition was also found once the V^{4+}/V^{5+} redox reaction occurred. Therefore the high-valence cation Ti^{4+} doping method was also presented and carefully studied, that leading to the largely improvement of electronic and ionic conductivity of NVP.[5] Thus it can be seen, the doping amount and the doping species could make effective impact on the electrochemical performance.

The high-entropy NVP was also synthesized very recently by Zhao et. al[6] with the formular $Na_3VAl_{0.2}Cr_{0.2}Fe_{0.2}In_{0.2}Ga_{0.2}(PO_4)_3$ (NVMP) which exhibited 102 mAh/g capacity and long-time lifespan at 20 C. Nevertheless the high-entropy doping successfully activated V^{4+}/V^{5+} redox reaction, the specific capacity of NVMP remains relative low due to the large amount of non-electrochemical active dopants elements in

the NVMP. Excess doping could hinder the crystallization of active material or destroy the stability of the crystal structure. This may lead to poor electrochemical performance.

According to S6-S7, different doping ratios were tested and the optimal performance was obtained for 0.1 high-entropy doping ratio. A comparison of all doped active and inactive element tests showed that the best results were obtained when doped active and inactive elements interacted.

High entropy Effect

Generally, for a random solid solution, the ideal configurational entropy (ΔS_{conf}) per mole can be given as[6]:

$$\Delta S_{conf} = -R\sum_{i=1}^{n} x_i \ln x_i$$

where R is the ideal gas constant and x_i represents the molar fraction of the ith component. For a good number of components n, the configurational entropy reaches the largest value when the atomic fraction is the same for all components (equimolarity). In this case, the configurational entropy per mole is:

$$\Delta S_{\text{conf}} = -R(\frac{1}{n}\ln\frac{1}{n} + \frac{1}{n}\ln\frac{1}{n} + ... + \frac{1}{n}\ln\frac{1}{n}) = R\ln n$$

Using the definition derived from statistical thermodynamics, the configurational entropy (ΔS_{conf}) of HE-$NV_{1.9}MP$ was calculated to be 0.279R and the conformational entropy of $Na_3V_2(PO_4)_3$ is 0.

Different from the low-entropy materials the advantages of high-entropy materials can be summarized as below:

High-entropy effect: According to the Gibbs-Helmholtz equation, the high entropy could help the material to alleviate the formation energy in the solid solution phase thus promote the formation/synthesis of the multiple-element structure.

Reduce the cation migration: In High-entropy battery materials, differences in neighboring atoms between crystal sites can increase the migration barrier for jump diffusion between these sites and reduce the cation migration in the compound therefore, the high entropy configuration could retard for the structure collapse and improve the stability of the materials. Moreover, this stable structure could sustained up Na^+ extraction/insertion thus helpful in the cycling performance.

Cocktail effect: As discussed in the material design part, different doping element could induce different advantage to the system. The co-doping high-entropy material could inherent

those advantage therefore electrochemical performance is influenced not only by the average properties of each doped element, but also by the effects of inter-element interactions[7].

In our work, the detailed cell volume parameters in Table S2 clearly confirm that the introduction of high entropy into the NVP accommodated lattice strain. The high entropy modification changed the lattice parameters of the material, in particular the c-axis became smaller, which would result in a smaller volume change after the phase transformation. Our calculations from the subsequent in situ XRD process induced a small volume variation of the $NV_{1.9}MP$ was 4.38%, markedly less compared to other extensively recorded NASICON-structured cathodes, like $Na_3V_2(PO_4)_3$ (8%)[8], $Na_3V_{1.5}Cr_{0.5}(PO_4)_3$ (6.8%)[9] and , $Na_3VMn(PO_4)_3$ (7.9%)[10]. And this small volume change was responsible for the high structural stability and long life cycle of HE-$NV_{1.9}MP$.

According to the results of CV and GITT, HE-$NV_{1.9}MP$ reduced the redox potential difference and the redox peak intensity was stronger compared to NVP, indicated that High entropy modification had reduced polarization and boosted Na^+ diffusion kinetics.

Table S1. Detailed structure information of $Na_3V_2(PO_4)_3$ from Rietveld refinement from the X-ray power diffraction pattern.

$Na_3V_2(PO4)_3$ sample. Rhombohedral symmetry, space group R-3c a=b=8.730 Å, c=21.823 Å, V=1440.461 $Å^3$
weighted profile R-factor, Rwp=6.96%, Rp=9.61%, X2=20.83

Atom	Wyckoff site	X	Y	Z	Occupancy
Na1	6b	0.3333	0.6667	0.1667	0.860
Na2	18e	0.6667	0.9710	0.0833	0.741
V	12c	0.3333	0.6667	0.0185	1.000
P	18e	-0.0424	0.3333	0.0833	1.000
O1	36f	0.1386	0.4977	0.0818	1.000
O2	36f	0.5520	0.8470	-0.025	0.998

Table S2. Detailed structure information of HE-$NV_{1.9}MP$ from Rietveld refinement from the X-ray power diffraction pattern.

HE-$NV_{1.9}MP$ sample. Rhombohedral symmetry, space group R-3c a=b=8.732 Å, c=21.799 Å, V=1439.685 $Å^3$
weighted profile R-factor, Rwp=6.77% , Rp=4.82%, X2=9.879

Atom	Wyckoff site	X	Y	Z	Occupancy
Na1	6b	0.3333	0.6667	0.1667	0.786
Na2	18e	0.6667	0.9644	0.0833	0.772
V	12c	0.3333	0.6667	0.0191	0.950
Ca	12c	0.3333	0.6667	0.0195	0.010
Mg	12c	0.3333	0.6667	0.0195	0.010
Cr	12c	0.3333	0.6667	0.0195	0.010
Ti	12c	0.3333	0.6667	0.0195	0.010
Mn	12c	0.3333	0.6667	0.0195	0.010
P	18e	-0.0460	0.3333	0.0833	1.000
O1	36f	0.1390	0.4963	0.0801	1.000
O2	36f	0.5539	0.8454	-0.025	0.980

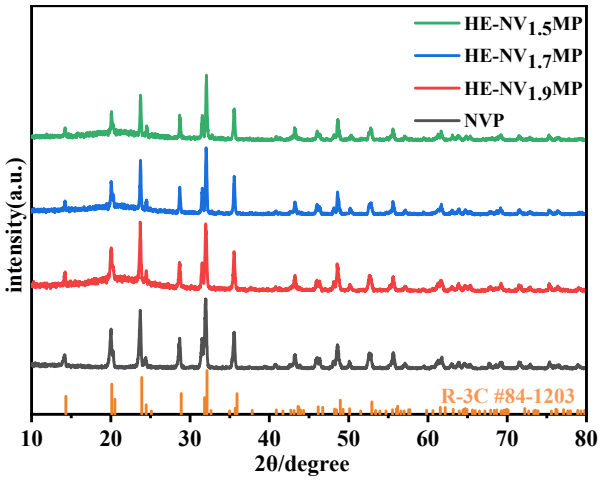

Fig. S1. (a)XRD patterns of $Na_3V_xM_{2-x}(PO_4)_3$ (x= 1.9, 1.7 and 1.5)

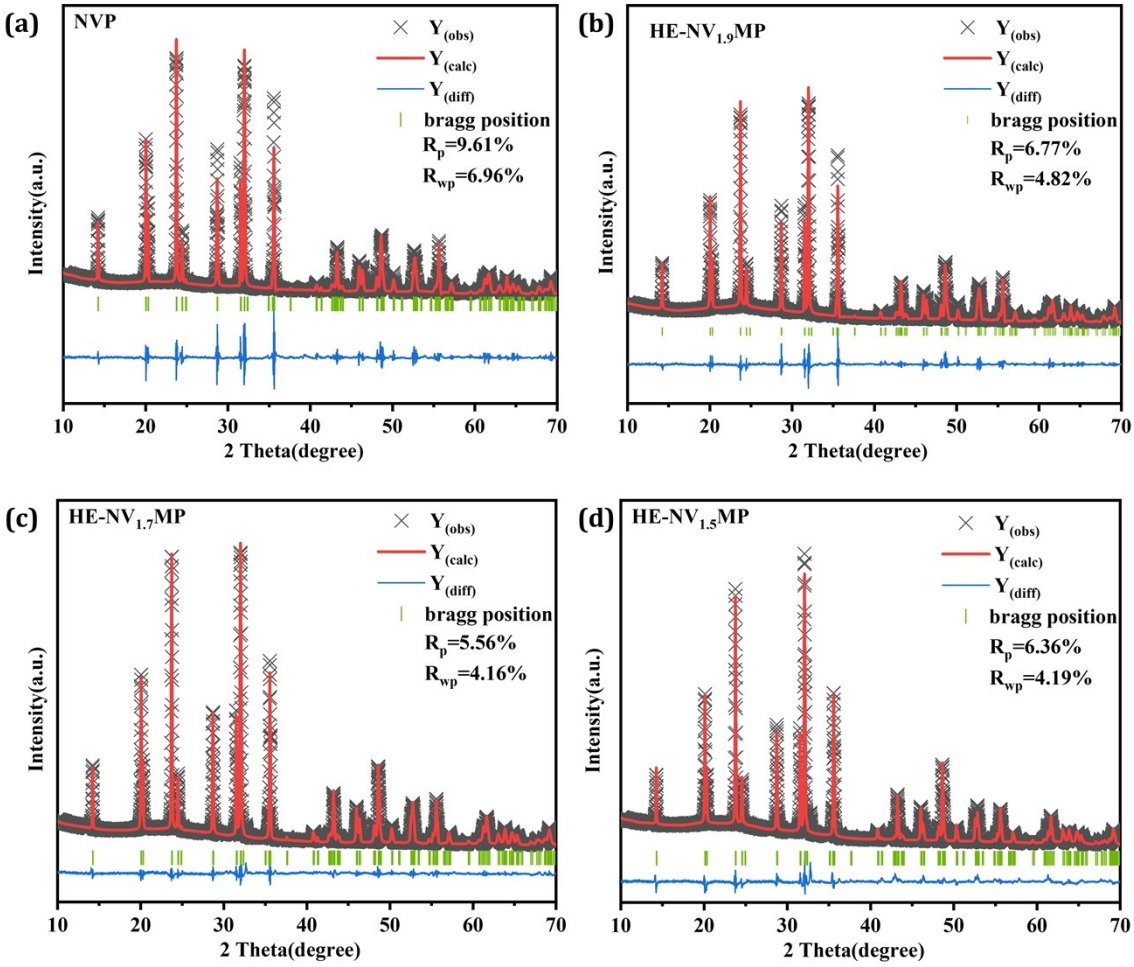

Fig. S2. XRD pattern and Rietveld refinement of NVP,HE-$NV_{1.9}$MP, HE-$NV_{1.7}$MP and HE-$NV_{1.5}$MP.

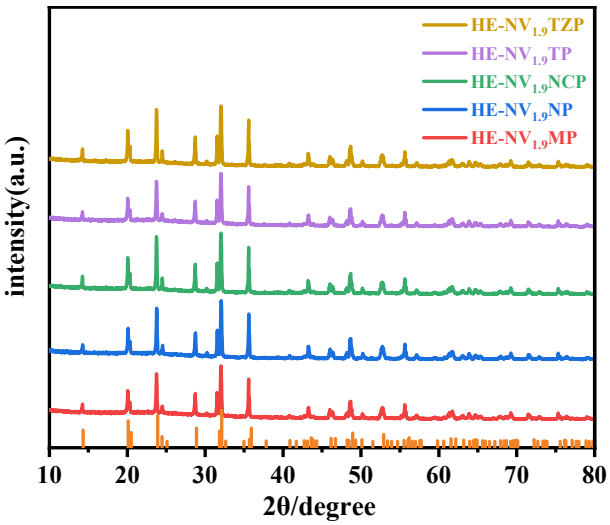

Fig. S3 XRD patterns of $Na_3V_{1.9}(Ca,Mg,Cr,Ti,Mn)_{0.1}(PO_4)_3$ (HE-$NV_{1.9}$MP), $Na_3V_{1.9}(Ni,Mg,Al,Cr,Mn)_{0.1}(PO_4)_3$ (HE-$NV_{1.9}$NP), $Na_3V_{1.9}(Ni,Co,Al,Cr,Mn)_{0.1}(PO_4)_3$ (HE-$NV_{1.9}$NCP), $Na_3V_{1.9}(Ca,Mg,Al,Ti,Mn)_{0.1}(PO_4)_3$ (HE-$NV_{1.9}$TZP), $Na_3V_{1.9}(Ca,Mg,Al,Ti,Zr)_{0.1}(PO_4)_3$ (HE-$NV_{1.9}$TZP).

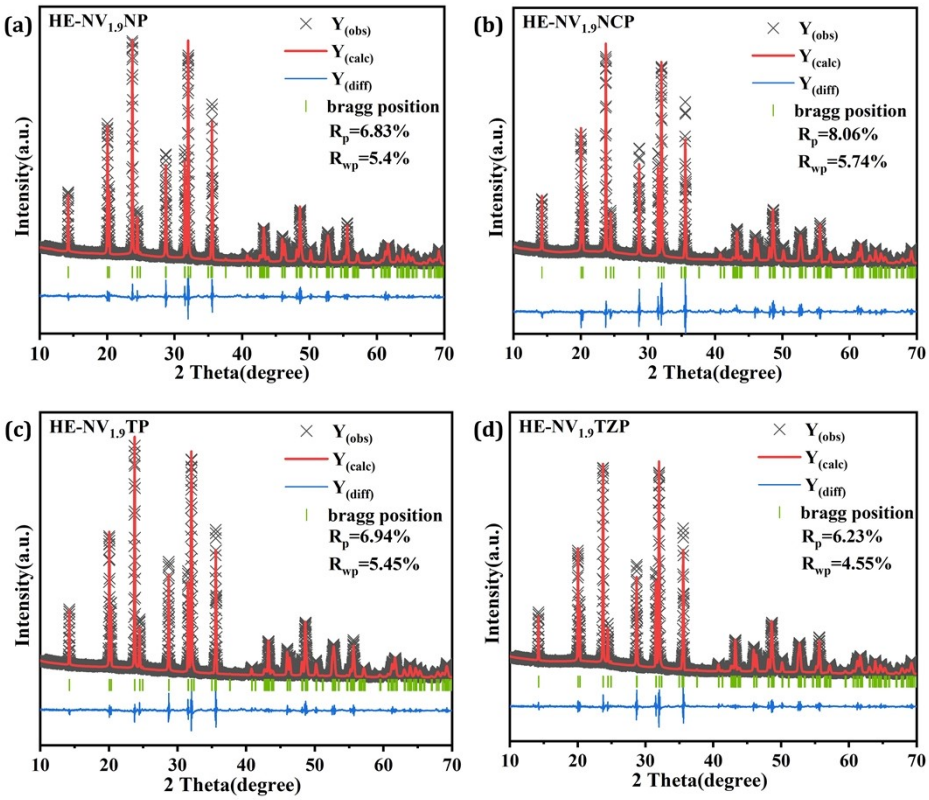

Fig. S4 XRD pattern and Rietveld refinement of HE-$NV_{1.9}$NP, HE-$NV_{1.9}$NCP, HE-$NV_{1.9}$TZP and HE-$NV_{1.9}$TZP.

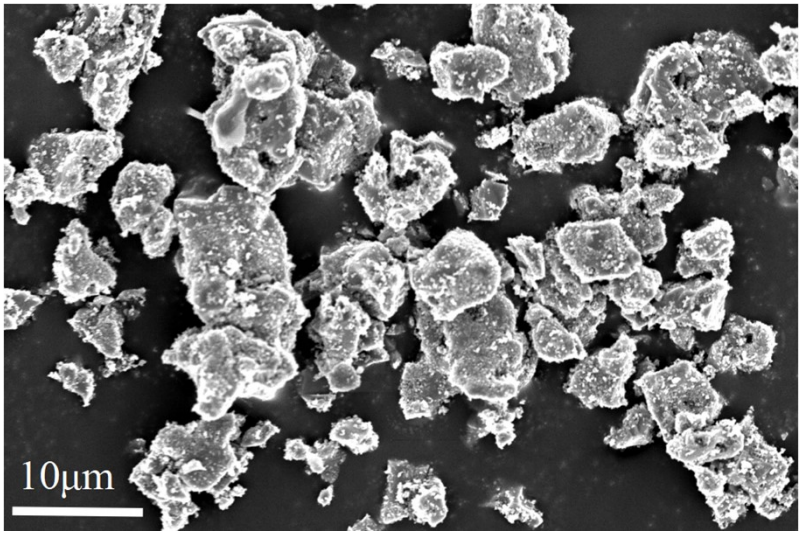

Fig. S5. SEM image of NVP

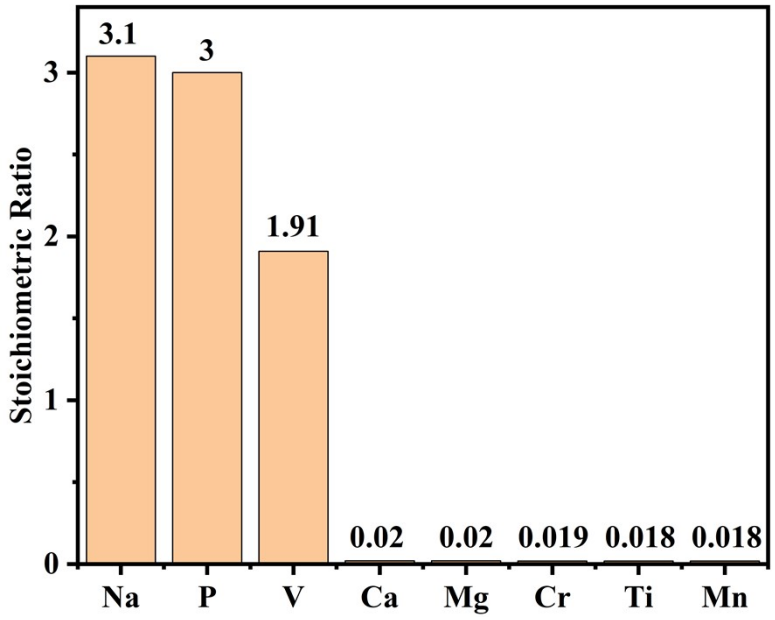

Fig. S6 Stoichiometric ratio of elements in HE-$NV_{1.9}MP$ by ICP-OES.

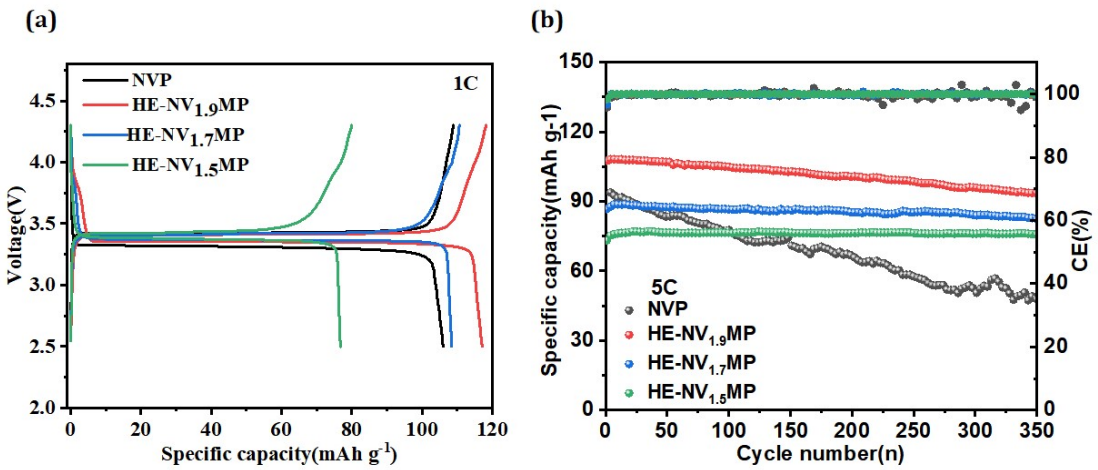

Fig. S7. (a)The initial charge-discharge curves in the voltage range of 2.5-4.3 V at 1 C (b) The cycling performances at 5C of $Na_3V_xM_{2-x}(PO_4)_3$ (x= 1.9, 1.7 and 1.5)

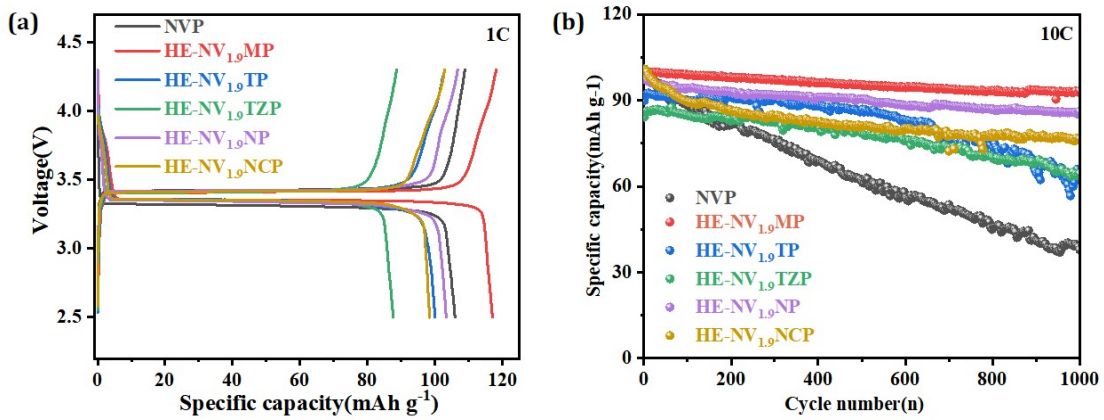

Fig. S8 (a) The initial charge-discharge curves in the voltage range of 2.5-4.3 V at 1 C (b) The cycling performances at 10C of NVP,HE-$NV_{1.9}$MP, HE-$NV_{1.9}$NP, HE-$NV_{1.9}$NCP, HE-$NV_{1.9}$TZP and HE-$NV_{1.9}$TZP.

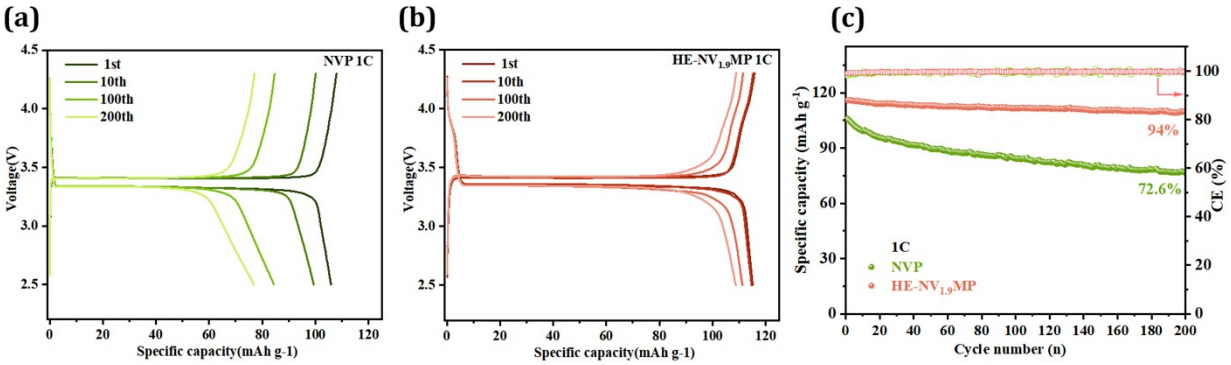

Fig. S9 Charge-discharge curves of the 200 cycles at 1 C of NVP(a) , HE-$NV_{1.9}$MP(b) and cycling performance comparison at 1 C.

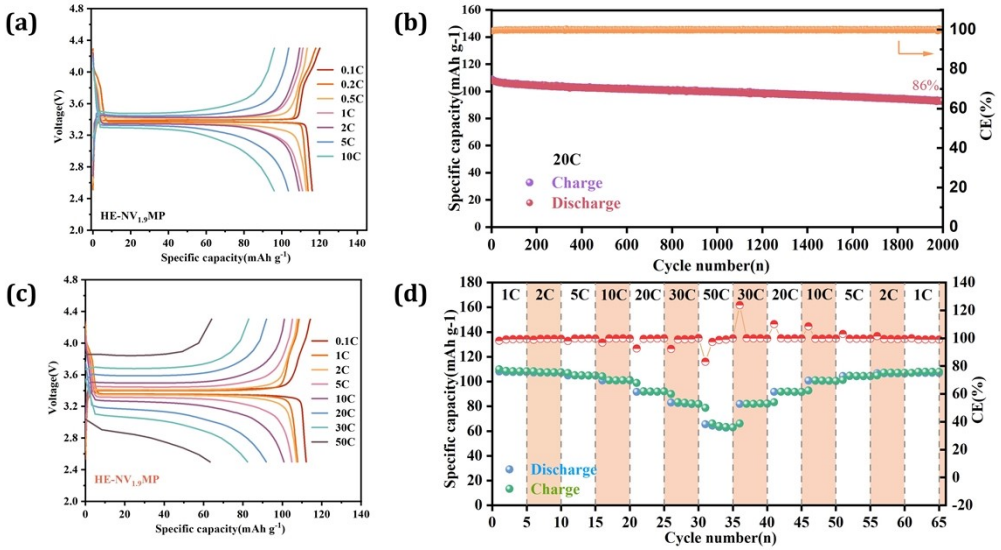

Fig. S10 (a)The charge-discharge curves of HE-$NV_{1.9}$MP at different current rates at Room temperature.(b) The rate performances of HE-$NV_{1.9}$MP at 50℃.(c) The charge-discharge curves and (d) rate capability of HE-$NV_{1.9}$MP at different current rates at 50℃.

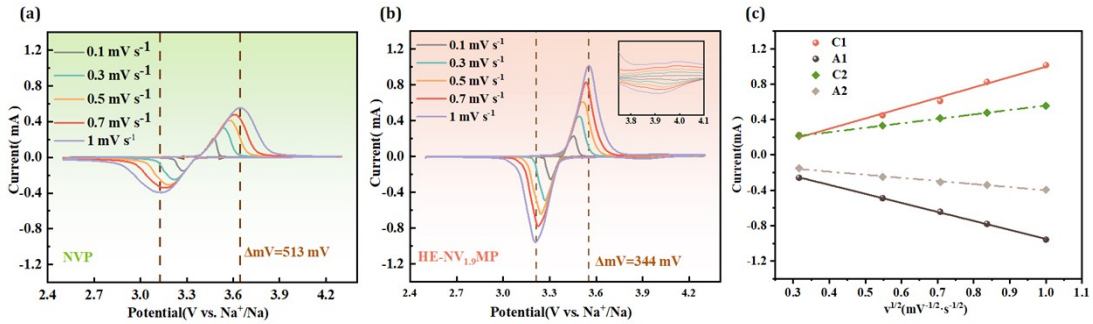

Fig. S11 CV curves of NVP(a) and HE-$NV_{1.9}$MP(b) in the voltage range of 2.5-4.3 V. (c) the linear fitting for the relationship between ip and v1/2 from the CV profiles of NVP (C2 and A2)and HE-$NV_{1.9}$MP(C1 and A1).

CV curves were recorded in a potential window of 2.5-4.3 V versus Na^+/Na at various scan rates from 0.1 to 1.0 mV s^{-1}. In the CV curves, the $D_{app,Na}$ values were calculated according to the following Randles-Sevcik equation:[7]

$$i_p=2.69\times10^5 n^{3/2} A D_{app,Na}^{1/2} C_0 v^{1/2}$$

where i_p is the peak current density, n is the electron-transfer number per molecule formula during the redox reaction (n = 2 for the NVP), A is the surface area of the electrode, C_0 is the concentration of Na ions in the electrode (7.7 mmol cm^{-3}), and *v* is the scan rate.

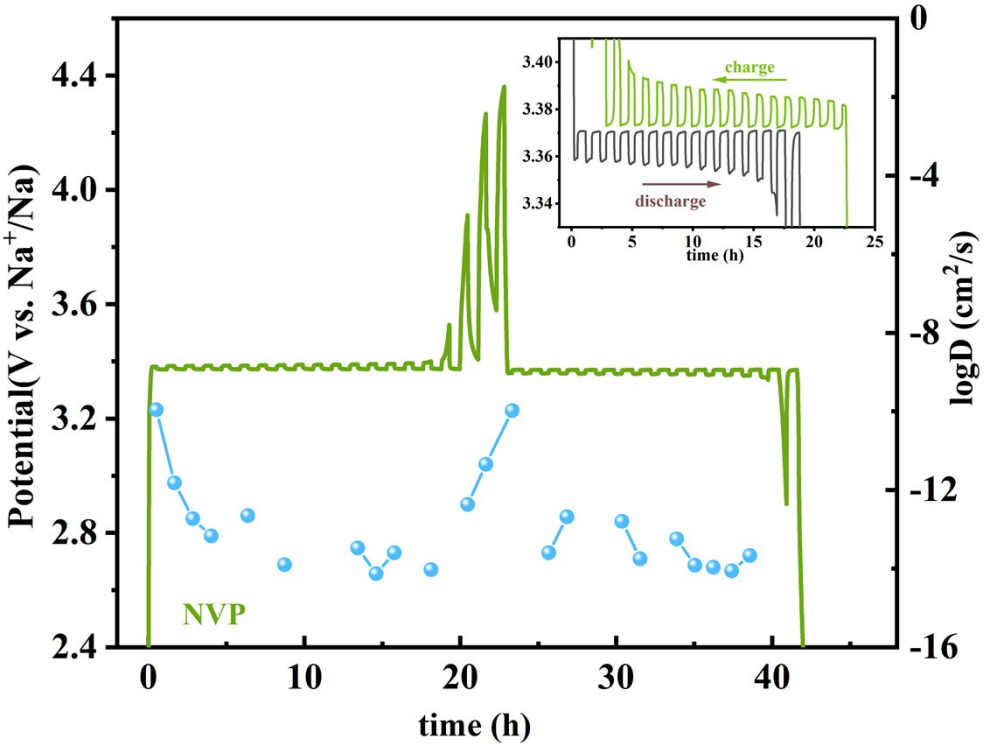

Fig. S12 (a) GITT measurement curves and the sodium-ion diffusion coefficient (log D_{Na^+}) of NVP.

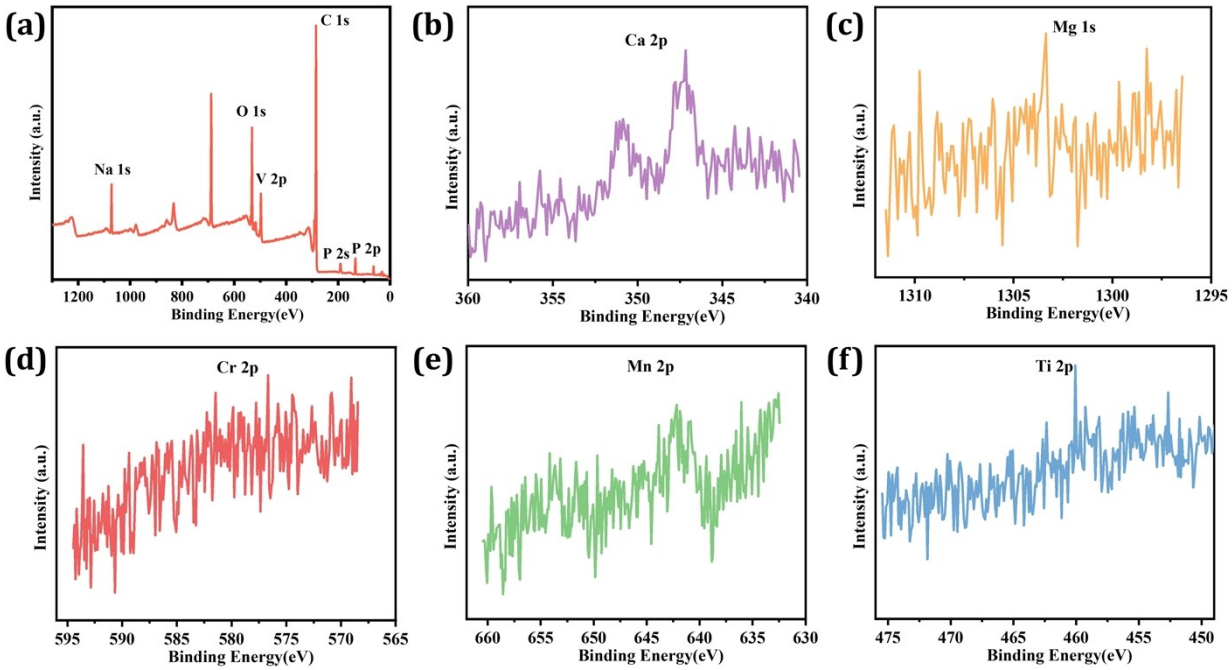

Fig. S13 high-resolution XPS spectra for the orbital peaks of Ca 2p, Mg 1s, Cr 2p, Mn 2p and Ti 2p.

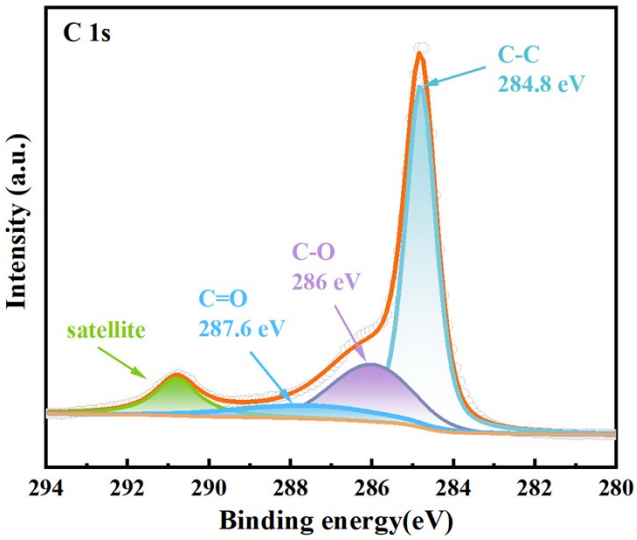

Fig. S14 high-resolution XPS spectra for the orbital peaks of C 1s.

The C1s of carbon is generally used as the reference peak for calibration. In our work, the difference between the measured peak and the reference peak (284.8 eV) was used as the charge correction value (Δ) to correct the binding energy of the other elements in the spectrum. We further complemented the C 1s spectrum of $NV_{1.9}MP$ with a figure showing three types of carbon peaks that belong to the C-C, C-O, and C=O bonds, respectively.(as can be found in the SI)

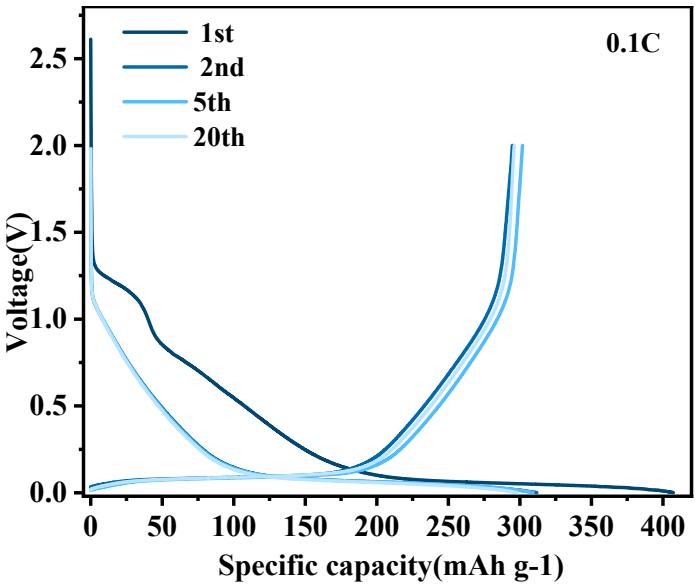

Fig. S15 Charge-discharge curves at 0.1 C of the HC anode in the half cell

Reference:

1. L. Zhao, H. Zhao, Z. Du, J. Wang, X. Long, Z. Li and K. Świerczek, *Journal of Materials Chemistry A*, 2019, **7**, 9807-9814.
2. M. Wang, Y. Tao, D. Zhang, G. Sun, P. Feng and C. Chang, Journal of Materials Science: Materials in Electronics, 2020, 31, 18360-18369.
3. J.-S. Park, J. Kim, J. H. Jo and S.-T. Myung, *Journal of Materials Chemistry A*, 2018, **6**, 16627-16637.
4. C. Xu, J. Zhao, Y.-A. Wang, W. Hua, Q. fu, X. Liang, X. Rong, Q. Zhang, X. Guo, C. Yang, H. Liu, B. Zhong and Y.-S. Hu, *Adv. Energy Mater.*, 2022, **12**, 2200966.
5. Y. Huang, X. Li, J. Wang, L. Miao, C. Li, J. Han and Y. Huang, *Energy Storage Materials*, 2018, **15**, 108-115.
6. M. Li, C. Sun, Q. Ni, Z. Sun, Y. Liu, Y. Li, L. Li, H. Jin and Y. Zhao, *Adv. Energy Mater.*, 2023, **13**, 2203971.
7. X. H. Rui, N. Ding, J. Liu, C. Li and C. H. Chen, *Electrochimica Acta*, 2010, **55**, 2384-2390.